Citation (APA)
Wang, H., Blauw, A., van Gils, J., Boelee, E., Sylvestre, E., & Medema, G. (2026). Modelling peak microbial pollution events caused by combined sewer overflows in a source-to-sea system. *Environmental Pollution*, *409*, Article 129053.
https://doi.org/10.1016/j.envpol.2026.129053

Environmental Pollution 409 (2026) 129053

Contents lists available at ScienceDirect

Environmental Pollution

journal homepage: www.elsevier.com/locate/envpol

Modelling peak microbial pollution events caused by combined sewer overflows in a source-to-sea system

Hao Wang [a,b,*], Anouk Blauw [a], Jos van Gils [a], Eline Boelee [a], Émile Sylvestre [b,c], Gertjan Medema [b,c]

[a] Deltares, 2600 MH, Delft, the Netherlands

[b] Water Management Department, Faculty of Civil Engineering and Geosciences, Delft University of Technology, Stevinweg 1, Delft, 2628 CN, the Netherlands

[c] KWR Water Research Institute, Groningenhaven 7, 3433 PE, Nieuwegein, the Netherlands

ARTICLE INFO

Keywords:
Peak microbial pollution
E. coli modelling
Source-to-Sea
Climate projection
Real-time forecasting

ABSTRACT

Predicting peak microbial pollution events in downstream coastal bathing waters caused by combined sewer overflows (CSOs) is essential for protecting public health. In urban areas, wastewater effluents, CSOs, and surface runoff can contribute to elevated microorganism loads to downstream waters. These pressures are likely to be intensified by growing population density and more frequent heavy rainfalls due to climate change. This study developed a process-based model to simulate *Escherichia coli* (*E. coli*) emissions, transport, and fate from the initial sources to coastal beaches. A three-year retrospective simulation (2017-2019) shows that *E. coli* concentrations in CSO discharges varied widely across the catchment (4.6 – 7.3 ($\log_{10}$ CFU 100 ml^{-1})). 99th percentile *E. coli* concentrations (4.0 ($\log_{10}$ CFU 100 ml^{-1})) at the inland water outlet were dominated by local CSO emissions, whereas 90th percentile *E. coli* concentrations (3.6 ($\log_{10}$ CFU 100 ml^{-1})) reflected cumulative upstream contributions from both CSO and effluent emissions. With the simulation accuracy of 89%, the model reliably reproduced the *E. coli* dynamics on the downstream beach and showed strong performance in representing peak concentrations based on Complementary Cumulative Distribution Function (CCDF) analysis. The process-based model enables quantitative tracking of source contributions and identification of pollution hotspots, providing support for mitigation measures. The study lays down a source-to-sea modelling framework for representing pollution transport across the aquatic continuum and provides a transferable tool for microbial pollution forecasting and climate adaptation planning.

1. Introduction

In the past half-century, spending leisure time on beaches during bathing season has increased in popularity (Grace et al., 2023). This requires a sufficient water quality for recreational purposes to ensure the health of bathers. However, the population and urban density along the coast are high and continue increasing (Barragán and De Andrés, 2015; Cosby et al., 2024), which poses a threat to the coastal environment. Microbial pollution from domestic and industrial wastewater can degrade water quality and increase health risks for bathers in adjacent beaches (Al Aukidy and Verlicchi, 2017). These risks are likely to increase in the future as climate change intensifies the frequency of heavy rainfall events (Derx et al., 2023; Semenza, 2020; Sterk et al., 2016).

Across Europe's ageing wastewater infrastructure (EurEau, 2016), urban expansion, population growth, and rising standards of living have increased hydraulic loading on existing combined sewer systems, many of which were initially designed for much smaller populations. As a result, the frequency and magnitude of CSO events have increased, leading to increased pollutant discharged to receiving waters (Perry et al., 2024). In addition to the domestic flow, increases in heavy rainfall frequency driven by climate change (Mohammed et al., 2021; Nie et al., 2009) and expansion of impermeable urban surfaces (Salerno et al., 2018), have increased the stormwater contribution to wastewater in combined sewers, thereby increasing CSO frequencies and spill volumes (Perry et al., 2024). Quantitative microbial risk assessment results (Sterk et al., 2016) indicated that infection risks in recreational waters downstream of CSOs are likely to rise in the future as a result of these combined social and climatic pressures.

Due to short timescale fluctuations in CSO discharge and microorganism concentrations, as well as the need for rapid event-based

* Corresponding author. Deltares, 2600 MH, Delft, the Netherlands.
E-mail addresses: h.wwang@tudelft.nl, hao.wang@deltares.nl (H. Wang).

https://doi.org/10.1016/j.envpol.2026.129053
Received 1 June 2026; Received in revised form 24 August 2026; Accepted 26 August 2026
Available online 28 August 2026

sampling, direct measurements of microorganism concentration during peak microbial pollution events are rare (Botturi et al., 2021). Additionally, monitoring microorganism transport across the entire water continuum — from sewer systems to coastal bathing waters — with sufficient frequency for early warning and water management purposes is costly and impractical. Therefore, using process-based models to simulate microorganism emission, fate, and transport throughout the initial sources to the ultimate receiving waters (so-called source-to-sea system) is an efficient and cost-effective solution for microbial pollution prediction in bathing waters (Lam and Ahmadian, 2024; Vermeulen et al., 2015; Zhang et al., 2018).

Most process-based models are applied at catchment scales and primarily focus on rural areas (Bougeard et al., 2011). Only a limited number of models have been implemented for real-time forecasting purposes in urbanised recreational waters (van der Meulen et al., 2024). Among these, emissions from CSOs are often neglected (Islam et al., 2018) or estimated using a simplified linear regression relationship between the microbial load and total CSO discharge (Locatelli et al., 2020; Ouattara et al., 2013; Thorndahl et al., 2024). To account for the complexity of CSO emissions and improve the simulation of peak pollution events in bathing waters, a modelling framework incorporating detailed sewer system representations and high-resolution rainfall inputs is required (van der Meulen et al., 2024).

Besides, the connection between upstream inland waters (Inland water means waters within the coastal boundary line) and downstream coastal waters is often overlooked in most existing models (Bravo et al., 2017; Chan et al., 2013; Eregno et al., 2018; Penna et al., 2023). As a result, the connections between upstream sources and coastal waters remain unclear. During transport from inland waters to the coast, various environmental factors continuously modify pollutant concentrations and distributions. Since the current modelling frameworks do not represent the hydrological and water quality continuity between inland and coastal waters, achieving systematic future projections of microbial pollution impacts remains challenging.

To quantify microbial pollution originating from short-term CSO events and its' impacts on the water quality of downstream coastal recreational waters, this study develops a generic source-to-sea modelling framework for predicting and projecting peak microbial pollution events across the aquatic continuum. The modelling framework integrates: 1) a coupled rainfall-runoff (RR) and emission model with detailed sewer representation to calculate *E. coli* pollution from sewerage; 2) a coupled hydrology and water quality model, and 3) a coupled hydrodynamic and water quality model to calculate the dilution, fate and transport of *E. coli* in inland surface waters and coastal waters, respectively. Unlike previous studies that focus on individual components of the system, the framework explicitly links microbial pollution emissions, inland transport processes, and coastal dynamics within a single modelling chain. Particular emphasis is placed on the validation of peak pollution events. In addition to conventional overall goodness-of-fit metrics, the ability of the model to reproduce peak events is evaluated against sit-specific *E. coli* monitoring data using complementary cumulative distribution functions. This comprehensive model validation can support both real-time forecasting and future climate change impact assessments, with applications to early warning, water quality management, and long-term adaptation planning.

2. Methodology

2.1. Study area

The Netherlands is situated in the delta of the Rhine and Meuse rivers, with extensive areas located below mean sea level. The Dutch ‘polder-boezem’ systems regulate inland water levels by pumping excess water from low-lying sub-catchments (polders) into canals (boezems) and ultimately discharging it to the sea (de Graaf et al., 2009; Van der Brugge et al., 2005). Rijnland Waterboard (Hoogheemraadschap van Rijnland) manages its inland water network with a total area of 1100 km^2 (Fig. 1a) and a population of 1.3 million. The system contains 17 wastewater treatment plants (WWTPs) and is hydraulically connected to the Rhine River, the North Sea, and neighbouring waterboard systems through five controlled hydraulic connections (Fig. 1b). Downstream of the inland water system is Katwijk (Fig. 1c), where the beaches are negatively influenced by WWTP effluents and CSOs (Belinda et al., 2016; Ing and der Meulen, 2007; Mattijs et al., 2008; Peter et al., 2023).

2.2. Coupled model setup

2.2.1. 1D inland water model

The inland hydrological model, consisting of a comprehensive urban drainage and sewer system and a detailed surface water network, was developed based on the Sobek 2 Suite. SOBEK 2 Suite is widely used for inland water quantity and quality studies, such as modelling salt intrusion in the Rhine-Meuse delta (Prinsen and Becker, 2011; Prinsen et al., 2015). The inland hydrological model consists of a rainfall-runoff component for sub-catchments (RR connections) and a flow component for canal networks (Fig. 1b). The rainfall-runoff component is a conceptual hydrological module that simulates runoff generation, infiltration, groundwater storage and drainage, evaporation and water exchange between saturated and unsaturated zones based on storage concepts and process-based flux calculations at sub-catchment scale. The generated runoff is subsequently routed through the canal network by the SOBEK 1DFLOW solver based on the one-dimensional Saint--Venant equations (Deltares, 2026).

The RR model is coupled with the D-emissions model, which calculates pollutant fluxes from various sources to surface water via different pathways (Deltares, 2023). In total, 808 sub-catchments contribute *E. coli* emissions to the canal network (Fig. 1). These sub-catchments are represented by four land use types: paved areas, unpaved areas, local surface waters, and WWTPs (Fig. S2).

Paved areas are characterised by their number of inhabitants, water consumption per capita, sewer capacity, and connections to WWTPs. Stormwater on the paved areas either flows overland to nearby local surface water or is collected by the sewer system and conveyed to the corresponding WWTPs. When sewage flow exceeds the sewer capacity, a CSO occurs at the connection between the sub-catchment and the canal network, discharging to the canal. Runoff from unpaved areas flows to groundwater and downstream local surface water. Local surface water receives rainfall directly and as runoff from paved and unpaved areas. Water management structures control water flow between local surface waters and canal networks to stabilise water levels (Fig. S2).

Given the high level of urbanisation in the study area, the main pollution source of the emission model is domestic wastewater (Servais et al., 2007). The *E. coli* concentration in CSO and effluent discharge at each timestep (10-min interval) is calculated in the model as follows

$$C_{EC,CSO} = \frac{pcL_{in} \times Inh \times 10000}{(Inh \times Q_{domestic} + Q_{col\_storm}) \times 86400} \tag{1}$$

$$C_{EC,effluent} = \frac{pcL_{in} \times Inh \times 10000}{(Inh \times Q_{domestic} + Q_{col\_storm}) \times 86400} \times 10^{-\mathrm{LRV}} \tag{2}$$

where, $C_{EC,CSO}$ and $C_{EC,effluent}$ (CFU 100 ml^{-1}) represent the *E. coli* concentration in CSO and effluent discharge, respectively, $Q_{domestic}$ and Q_{col_storm} represent the water consumption per capita (m^3 cap^{-1} s^{-1}) and collected stormwater discharge (m^3 s^{-1}), respectively. *Inh* (cap) is the number of inhabitants on the paved area. pcL_{in} is a constant per capita emission rate (CFU cap^{-1} d^{-1}). LRV represents the *E. coli* log removal value of WWTPs. The factors 86400 and 10000 are unit conversion constants, corresponding to seconds per day and cubic meters to 100 mL, respectively.

Here, pcL_{in} and LRV are set as 3.61×10^{10} CFU cap^{-1} d^{-1} and 2.05, respectively (van Heijnsbergen et al., 2022). Observations at the

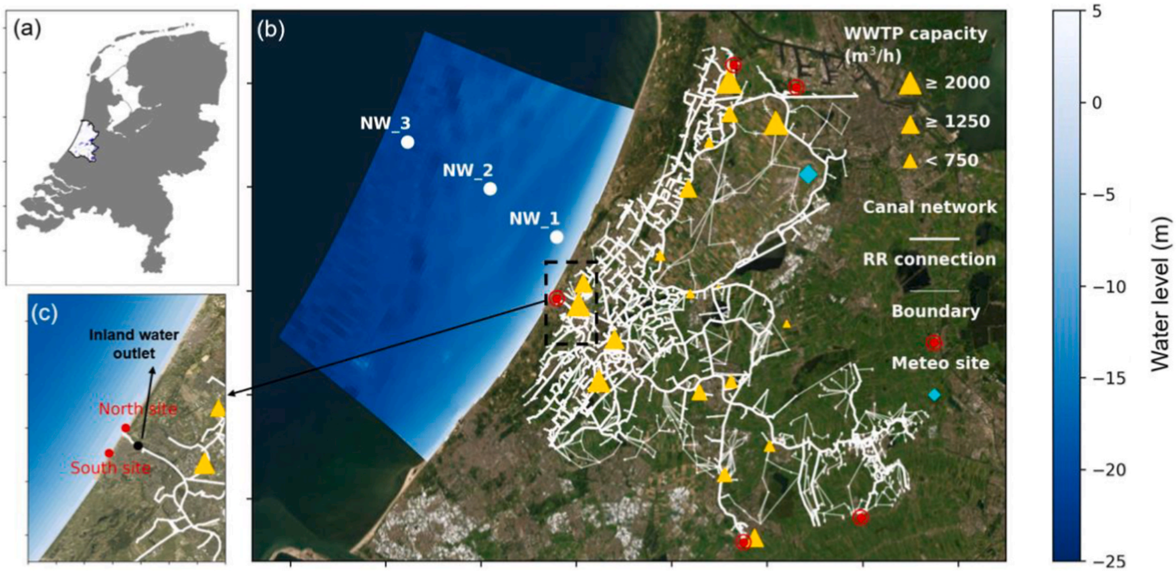

Fig. 1. The coupled model domain. (a) Location of the study area. (b) Model domain with Rainfall-runoff (RR) connections, cancel networks, WWTPs and boundaries of the inland water system, monitoring stations for seawater temperature, salinity and suspended sediment (white circles), and a meteorological site for precipitation input (cyan diamond). Hourly discharge time series used as boundary conditions at these boundaries are shown in Fig. S1. (c) Locations of the *E. coli* monitoring stations at the beach and the inland water outlet. (For interpretation of the references to colour in this figure legend, the reader is referred to the Web version of this article.)

Dutch-German border (van Heijnsbergen et al., 2022) show that LRV decreases from 3.05 to 2.05 as influent water volumes increase, reflecting a reduced treatment performance under higher hydraulic loading. We therefore adopt 99.1% as a conservative assumption for wet weather conditions.

E. coli load from CSOs ($L_{EC,CSO}$) is influenced by sewer capacities ($V_{full\_capacity}$, m^3) and the current water volume in the sewer ($V_{sewer,t-1}$, m^3)):

$$L_{EC,CSO} = Q_{CSO} \times C_{EC,CSO} \tag{3}$$

$$Q_{CSO,t} = \max\left(0, \frac{V_{sewer,t-1} + \left(Inh \times Q_{domestic} + Q_{col_{storm},t} - Q_{out,t}\right) \times \Delta t - V_{full_{capacity}}}{\Delta t}\right) \tag{4}$$

Q_{out} and Q_{CSO} represent sewer outflow discharge (m^3 s^{-1}) and CSO discharge (m^3 s^{-1}), respectively. These are calculated by the RR model based on precipitation input. Model inputs on the locations of effluents and CSO outfalls, inhabitant distribution, sewer capacity and connections between WWTPs and paved areas were provided by the water board. The meteorological inputs, including 10-min precipitation data and hourly evaporation data, were downloaded from the Royal Netherlands Meteorological Institute website (https://dataplatform.knmi.nl/dataset/) at Schiphol (Fig. 1b).

After receiving water discharges from the RR connections, the flow velocities and directions in the canal network were calculated based on the water balance. Five hydraulic boundaries (Fig. 1b) control water exchange between the studied inland water system and adjacent water bodies. Hourly discharge data, measured at these stations by the waterboard, were used as model boundary conditions (Fig. S1), while hourly water level observations within the canal network were used for hydrological model validation (Fig. S3).

The dilution, fate and transport of *E. coli* in the canal network are simulated by the water quality model, which considers *E. coli* die-off driven by temperature, salinity, and UV radiation, and sediment interactions, including attachment, detachment, sedimentation, resuspension, and hyporheic exchange (Wang et al., 2025). Details of the process equations and parameter values are provided in the **SI text** and Table S1. However, interaction between *E. coli* and suspended sediment in inland waters was excluded due to insufficient data on sediment dynamics. Time series observations of temperature and radiation at De Bilt (52°05′56.0″N 5°10′46.9″E) are from the Royal Netherlands Meteorological Institute (https://dataplatform.knmi.nl/dataset/). The long-term average monthly DOC concentration dynamics without spatial variations are calculated based on the observations of 90 stations spread across the whole of Rijnland area, from the Waterkwaliteitsportaal (https://wkp.rws.nl/downloadmodule), and are applied to calculate the UV extinction coefficient (following the approach as described in Wang et al., 2025).

2.2.2. 3D coastal water model

The 3D model for coastal waters (Fig. 1b) is nested within the Dutch continental shelf model (DCSM), which is developed based on the Delft3D FM Suite 2D3D (Deltares, 2022). Delft3D FM solves the shallow water equations on an unstructured (flexible) mesh and forms the hydrodynamic core of the DCSM, an advanced 3D model for the computation of water level, current, salinity, temperature, sediment, and water quality in the greater North Sea (Grasmeijer et al., 2022; Zijl et al., 2021; Zijl et al., 2015). The 3D coastal model covers an area 20 km north and south of the inland water outlet (pumping station; Fig. 1c) along the coastline and 20 km offshore (Fig. 1b). The spatial resolution is approximately 200m. The computational timestep of the model is 1 h.

The hourly open boundary conditions for hydrodynamics, including temperature, salinity, water level, and velocity, are provided by the DCSM model. Hourly meteorological inputs are from ERA5 (https://cds.climate.copernicus.eu/datasets). The water quality model in the 3D coastal model is the same as the 1D inland model, but adapted to 3D simulations. To calculate the interaction with sediment, we use the weekly dynamics of suspended sediment concentration on the boundaries from (Beyaard et al., 2025). The temporally varying DOC concentration input is the average value of observations from three monitoring stations (NW_1, NW_2, NW_3, Fig. 1b) from the MWTL monitoring programme of Rijkswaterstaat (https://waterinfo.rws.nl/). The temperature and salinity validation data are from the same monitoring programme. The *E. coli* monitoring data from the north and south stations on the beach (Fig. 1c) are from the National Georegister (https://www.nationaalgeoregister.nl/).

2.3. Model validation

2.3.1. Traditional validation

The coupled model simulation covered three years from 2017 to 2019, as the *E. coli* observations on the beach indicate high microbial pollution in these years (Fig. S4). The model performance in simulating inland water levels and water temperature, salinity, suspended sediment and *E. coli* concentration in coastal waters is evaluated by comparing with observational data. The metrics for validation are Root Mean Square Error (RMSE), normalised Root Mean Square Error (normalised-RMSE), and coefficient of determination (R^2).

2.3.2. Policy-oriented validation

In addition to the traditional model validation metrics, a policy-oriented validation was conducted to indicate whether or not events exceeding the regulatory threshold were simulated correctly. We established a binary classification of positive (>500 CFU 100 ml^{-1}) and negative (≤500 CFU 100 ml^{-1}) based on the threshold introduced by the European Bathing Water Directive (EU, 2006) for the long-term sufficiency of coastal bathing waters. Model performance in detecting pollution events was then described as true or false by comparing simulated and observed classifications. The statistics were calculated from the confusion matrix, which summarises the number of simulated classes and observed classes. Simulation accuracy rate is represented by the diagonal of the matrix:

$$\textit{Simulation accuracy rate} = \frac{\textit{True positives} + \textit{True negatives}}{N} \times 100\%$$

Where N represents the total number of predictions compared to truth values. True positives and true negatives represent correctly predicted exceedances and non-exceedances, respectively.

To represent the model performance for accurately predicting pollution events, we additionally calculate the alarm accuracy rate:

$$\textit{Alarm accuracy rate} = \frac{\textit{True positives}}{(\textit{True positives} + \textit{False negatives})} \times 100\%$$

Where false negatives represent cases where the observations indicate exceedance of the threshold, but the model fails to reproduce that.

2.3.3. Validation of the upper tail behaviour of the empirical distribution

The empirical complementary cumulative distribution function (CCDF) represents the probability that a concentration exceeds a given value and is commonly used in microbial risk assessment (Smeets et al., 2010). In this study, CCDF curves were constructed for both observed and simulated *E. coli* concentrations to compare their upper tail probabilities. To represent independent and identically distributed (i.i.d.) randomness and ensure a sufficiently large sample size, we collected observational samples at biweekly intervals from a longer period (2009 – 2024) as input. Given that the observational dataset during the simulation period does not adequately capture the upper tail of the distribution and the comparison focuses on distributional properties rather than temporal correspondence, the observations and simulation results with different time frames should be comparable.

2.4. Contributions of *E. coli* pollution sources

To identify the contributions of different *E. coli* pollution sources, the relative contributions of CSOs and effluents were calculated for periods when the *E. coli* concentrations at the inland water outlet exceeded the 90th percentile and 99th percentile thresholds. These ratios were derived using simulated *E. coli* loads from four effluents and eight CSO outfalls close to the beach.

3. Results and discussion

3.1. Evaluation of model performance and application

Downstream discharge is a commonly used metric for hydrological model validation. However, in this study, the 1D hydrology model incorporates a substantial proportion of pressurised flow, due to the characteristics of the Dutch surface water system. Consequently, water level dynamics are more representative for model validation than water discharges. The annual average observed water level in the canal network was approximately 3.36m relative to the canal bottom and −0.64m relative to the mean sea level, which is well reproduced by the model simulation (Fig. S3). The RMSE and normalised RMSE values of hourly water levels indicate that the 1D model provides reliable hydrology prediction (Table 1).

The 3D hydrodynamic model performance was validated by temperature (Fig. S5) and salinity (Fig. S6). Validation results indicate a strong model performance in the hydrodynamics simulation (Table 1). In contrast, model performance for suspended sediment was weaker; however, the model still captured the overall seasonal variability (Fig. S7).

The model validation of *E. coli* concentrations at the beach using standard statistical metrics, with an R^2 of 0.51 and RMSE value of 0.64 (log_{10} CFU 100 ml^{-1}) (Table 1), indicates an acceptable model performance. Process-based models are more commonly applied to rural catchments than urban systems for *E. coli* simulation. Urban watersheds have more complex wastewater and stormwater infrastructure and highly variable sources of *E. coli* compared to rural catchments, resulting in a lower predictability of *E. coli* (Chen and Chang, 2014; van der Meulen et al., 2024). In contrast, data-driven models have demonstrated strong performance in microbial pollution forecasting. R^2 values for state-based Bayesian, linear regression and random forests models range from 0.07 to 0.42 (Seis et al., 2024). RMSE values from the 3 corresponding data-driven models, trained on low-frequency sampling data without peak events, range from 0.58 to 1.01 (log_{10} CFU 100 ml^{-1}) (Seis et al., 2024), while models trained on high-frequency sampling data yield RMSE values in a range of 0.33 - 1.32 (log_{10} CFU 100 ml^{-1}) (Searcy and Boehm, 2021). Overall, the performance of the coupled process-based model in this study is good compared to data-driven models.

Policy-oriented model validation was assessed using simulation accuracy and alarm accuracy rates. During the bathing seasons across the simulation period, the microbial water quality at the beach was monitored on 95 days, of which 85 days were correctly classified by the model (Table 2), yielding a simulation accuracy rate of 89%, which is comparable with the reported data-driven models (90 - 96% for Bayesian belief network, 56 – 74% for Naïve Bayes, 60 - 79% for logistic regression and 67 – 81% for random forest (Panidhapu et al., 2020)), In total, observed positives were 28 days, of which 20 days were simulated positives, resulting in an alarm accuracy rate of 71%. Most missed alarms correspond to days when simulated *E. coli* concentrations were elevated relative to adjacent periods but did not exceed the threshold (Fig. 2).

Table 1
Indicators for *E. coli* prediction performance.

	RMSE	Normalised RMSE	R^2
Water level	0.12 m	3.6%	-
Temperature	1.0 °C	8.2%	0.98
Salinity	1.9 psu	6.2%	-
Suspended sediment	11.5 mg l^{-1}	83.9%	0.01
E. coli	0.64 (log_{10} CFU 100 ml^{-1})	33%	0.51

*Note: Due to the limited variability in water level and salinity, R^2 does not adequately reflect the model's prediction performance. Therefore, scatter plots were added in Figure S3 and Figure S8 to better illustrate the agreement between observed and simulated values of these variables.

Table 2
Confusion matrix for *E. coli* prediction performance.

	Simulated positives	Simulated negatives
Observed positives	20 (true)	8 (false)
Observed negatives	2 (false)	65 (true)

The comparison of observed and simulated *E. coli* ECCDF curves (Fig. 3) showed that the model reproduced exceedance probabilities more accurately at higher concentrations (above 200 CFU 100 ml^{-1}) than at low concentrations. RMSE and R^2 tend to reflect average performance and do not explicitly evaluate the frequency or magnitude of extreme pollution events. For risk-based water quality assessment, accurate representation of peak *E. coli* concentration and exceedance probabilities is critical. This limitation is therefore well addressed by using CCDF analysis in our study.

3.2. Understanding of E. coli dynamics

3.2.1. Variability and sources in the inland water system

Simulated *E. coli* concentrations and loads at the inland water outlet (Fig. 4) revealed several peaks. Variability in *E. coli* loads was primarily driven by variability in concentrations rather than water discharges. The 90th and 99th percentiles of *E. coli* concentrations at the inland water outlet were 3.6 and 4.0 ($\log_{10}$ CFU 100 ml^{-1}).

We use the above 90th percentile and 99th percentile exceedances to analyse the spatial distributions in inland waters. The spatial distributions of the duration of 90th percentile and 99th percentile exceedances exhibited different patterns (Fig. 5). The duration of 99th percentile exceedances shows a fragmented spatial pattern, forming three distinct clusters in the northern, western and eastern regions. Areas with high durations of 99th percentile exceedances were concentrated near CSO outfalls, suggesting that these 99th percentile exceedances were

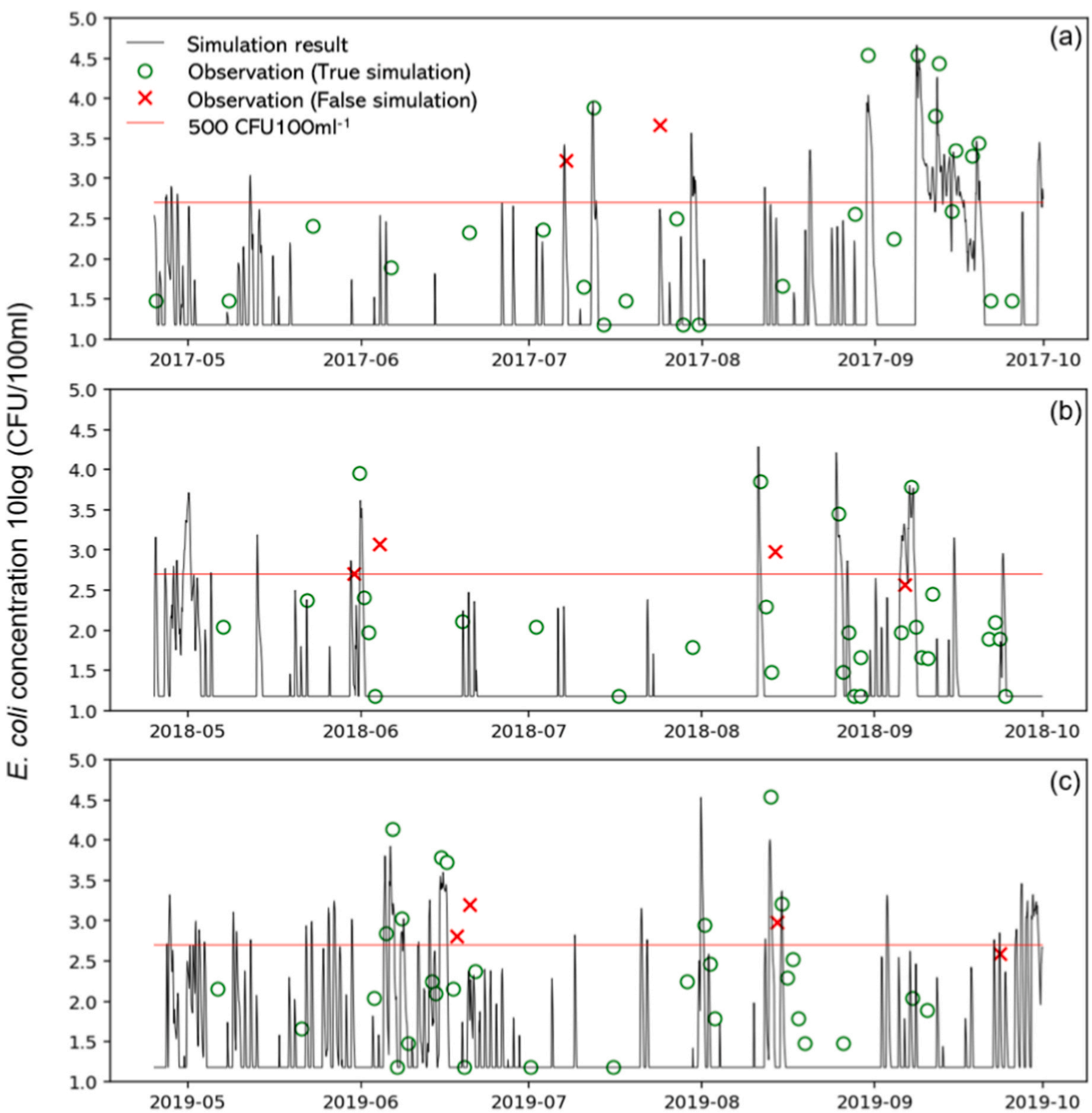

Fig. 2. Policy-oriented validation on the beach in 2017 (a), 2018 (b) and 2019 (c). The red line indicates the threshold (500 CFU 100 ml^{-1}) of the EU bathing water directive. The grey line depicts the modelled *E. coli* concentrations at the beach. The circles and crosses represent the observed *E. coli* concentrations, where circles represent situations where the model correctly predicted whether *E. coli* concentrations are above or below the threshold (True simulation), and crosses represent situations where the model did not predict this correctly (False simulation). (For interpretation of the references to colour in this figure legend, the reader is referred to the Web version of this article.)

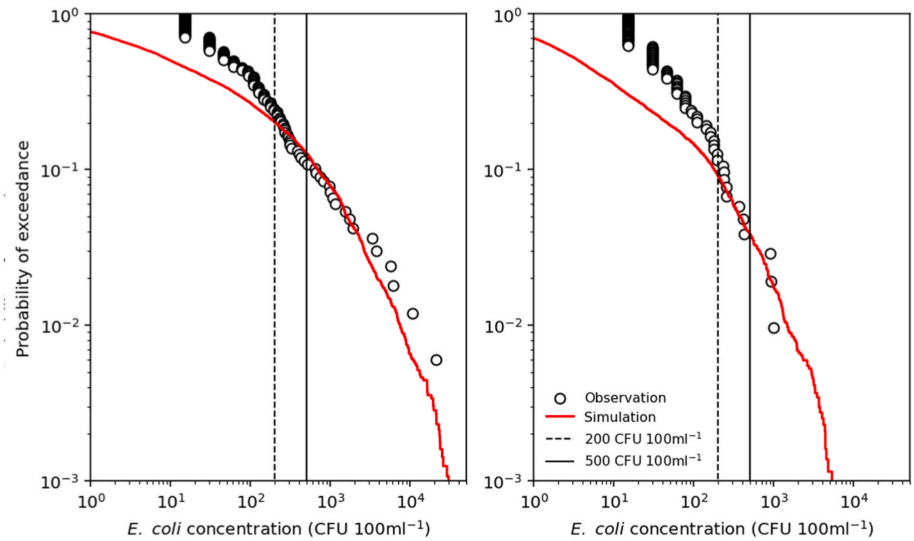

Fig. 3. Empirical complementary cumulative distribution function (ECCDF) curves of the observed (2009 – 2024) and simulated (2017 – 2019) *E. coli* concentrations in the north side (a) and south side of the beach (b).

primarily driven by local CSO discharges with limited spatial influence (Fig. 5a). In contrast, the duration of 90th percentile exceedances (Fig. 5b) exhibited a broader spatial extent, with additional influence observed near effluent discharge points.

Over the three-year simulation period, simulated *E. coli* concentrations in effluents ranged from 2.8 to 5.6 ($\log_{10}$ CFU 100 ml^{-1}) with an average of 4.2 (Fig. 5c). According to a two-year sampling campaign at 11 WWTPs along the German-Dutch border (2022), effluent *E. coli* concentrations were reported in a range of 2.66 - 5.77 ($\log_{10}$ CFU 100 ml^{-1}), The simulated *E. coli* concentrations in this study are in line with the reported range, supporting the reliability of the model prediction.

The simulated *E. coli* concentrations in CSOs were approximately two orders of magnitude higher than those in effluents, ranging from 4.6 to 7.3 ($\log_{10}$ CFU 100 ml^{-1}) with an average of 6.3 ($\log_{10}$ CFU 100 ml^{-1}) (Fig. 5a). Previous studies (Erichsen et al., 2006; Thorndahl et al., 2024) estimated *E. coli* concentrations of 6.4 ($\log_{10}$ CFU 100 ml^{-1}) using a weighted average of raw wastewater and stormwater contributions in Denmark. The geometric mean value reported by Servais et al. (2011) in the Paris area is 6.7 ($\log_{10}$ CFU 100 ml^{-1}). Passerat et al. (2011) observed the peak *E. coli* concentrations of 6.8 ($\log_{10}$ CFU 100 ml^{-1}) during the first 30 min of CSO discharge into the Seine River, followed by a rapid decline to 5.6 ($\log_{10}$ CFU 100 ml^{-1}). Similarly, Al Aukidy and Verlicchi (2017) reported a wide range of *E. coli* concentration in CSOs (1 to 7 ($\log_{10}$ CFU 100 ml^{-1})) based on observations from five outfalls in northeast Italy. Overall, the simulated average *E. coli* concentration in CSO outfalls in this study is in the same order of magnitude as reported in previous studies, with comparable ranges. Both our simulation results and previous observations indicate a large variation of *E. coli* concentration in CSOs. This suggests that using a constant concentration to simulate CSO pollution may be insufficient. Although further validation of our model is needed, it provides a complementary dataset to observations of *E. coli* dynamics in CSO discharges.

The ratios of *E. coli* load from CSOs and effluents, adjacent to the inland water outlet (black circle in Fig. 5a), during the 99th and 90th percentile exceedances were calculated to identify the contributions of pollution sources. During the 99th percentile exceedances, the average ratio between total loads from CSO and from effluents is 73 (Fig. 5d). Passerat et al. (2011) estimated that the CSO discharges approximately 79 times more *E. coli* than WWTPs, and can increase the downstream *E. coli* concentration 7-9 times higher than the upstream. Consistent with these findings, our simulation yields a similar CSO-to-effluent *E. coli* load ratio in 99th percentile exceedances, underscoring the dominant role of CSOs in driving 99th percentile exceedances in the inland water system. In contrast, during 90th percentile exceedances, these ratios were much lower, ranging from 0 to 8. The low CSO-to-effluent *E. coli* load ratio in 90th percentile exceedances and the continuous spatial distribution (Fig. 5a) suggested that effluents contribute substantially to more frequent, lower-intensity 90th percentile exceedances over broader spatial scales due to the cumulative downstream transport effects (Jalliffier-Verne et al., 2016).

3.2.2. Variability in the coastal water

The model identified 11, 13, and 23 pollution events (classified by exceedance of 500 CFU 100 ml^{-1}) at the northern beach during the bathing seasons of 2017, 2018, and 2019 (Fig. 3), respectively, with cumulative event durations of 310, 141, and 202 h. The shape and spatial extent of the pollution plumes varied between years, with the largest plume occurring in 2017 (Fig. 6). In addition, the plumes extended further northward than southward. The pollution area and duration indicated the highest risk in 2017 compared to the other two years. This is highly related to the *E. coli* load from the inland water, as the most frequent 99th and 90th percentile exceedances were detected at the inland water outlet. Notably, annual precipitation in 2017 was the highest among the simulation period and higher than the 30-year average (Fig. S9). This highlights the linkage between rainfall, CSO discharge and pollution on the downstream beach in the model.

Although the linkage is evident, the relationship between inland sources and beach pollution is complex. Model results show that the relationship between *E. coli* loads from the inland water outlet and *E. coli* concentration at the northern beach is weak, with the coefficient of determination below 0.05. Besides, different inland pollution loads result in varying pollution duration times at the beach. Discharge during 90th percentile exceedances resulted in short-lived beach pollution ($\leq$ 10 h), whereas discharge during 99th percentile exceedances produced substantially longer impact, with an average duration of approximately 37 h. Overall, pollution effects are larger on the northern side of the beach than on the southern side, aligning with the predominantly south-to-north nearshore current (Grasmeijer et al., 2022; Zijl et al., 2015; Zijl et al., 2013). Hence, the pollution events on the beach are tightly related to both the level of pollution discharge from inland sources and local hydrodynamic conditions, highlighting the importance of modelling microbial pollution in an aquatic continuum.

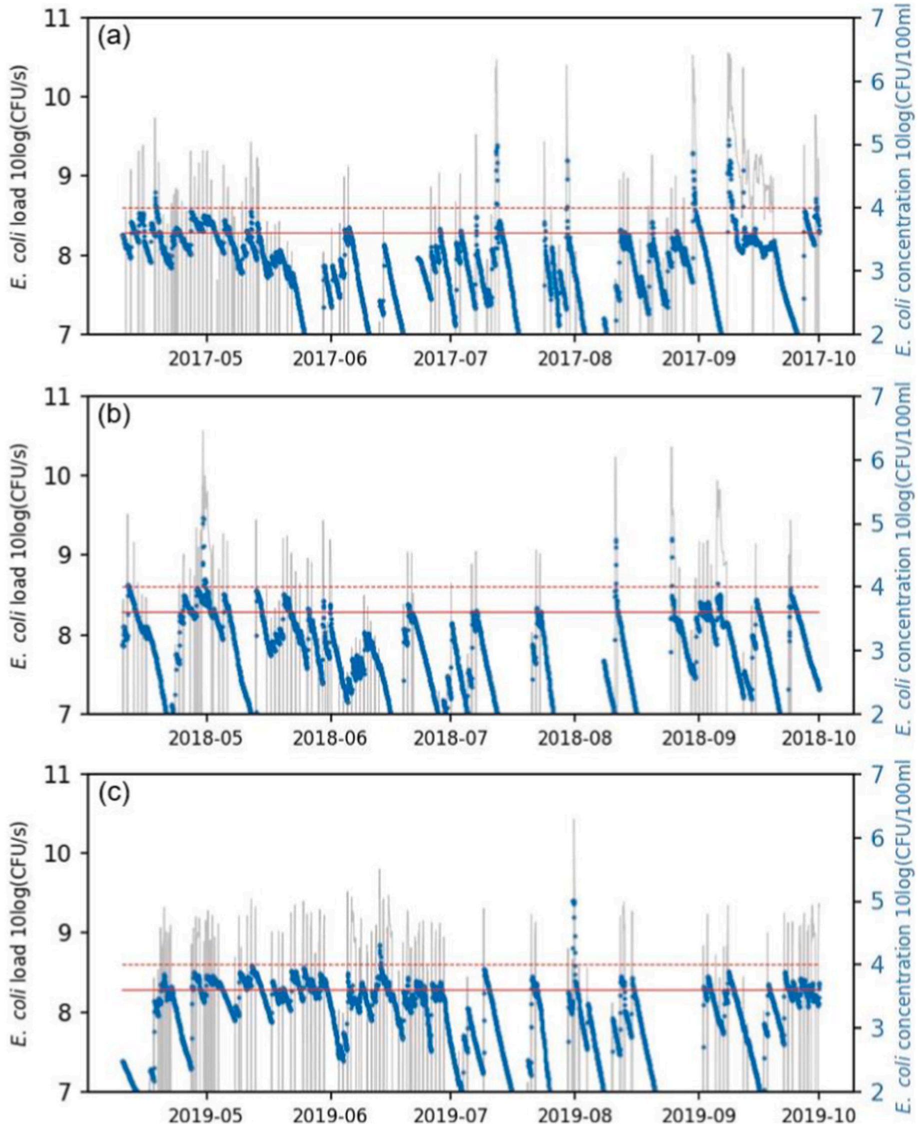

Fig. 4. Simulated *E. coli* concentrations (blue dots) and loads (grey lines) at the inland water outlet in 2017 (a), 2018 (b), and 2019 (c). The red solid line and red dashed line represent the 90th percentile and 99th percentile of the simulated *E. coli* concentrations, respectively. (For interpretation of the references to colour in this figure legend, the reader is referred to the Web version of this article.)

3.3. Implications and limitations

To facilitate forecasting applications, the coupled model was designed to require updates only to meteorological input variables and population density. Notably, the coupled model was applied without site-specific calibration, demonstrating that this knowledge-driven, process-based framework can serve as a generic approach for other urbanised coastal systems. Compared with data-driven models, process-based models do not require training datasets, and the model performance is not constrained by the size or quality of the training dataset. In addition, the process-based model provides detailed spatio-temporal information and enables the analysis of pollution sources and transport pathways to support decision-making and water quality management. On the other hand, observational data remain essential for model validation. Compared to the simulation accuracy rate, the relatively low alarm accuracy rate and the mismatch between ECCDF curves at low concentrations likely result from missing pollution sources in the model, including diffuse sources from agricultural areas, potential misconnected sewers, and direct inputs from pets, birds and tourists on the beach (Devane et al., 2020; Ellis and Butler, 2015).

For the *E. coli* simulation in effluents and CSOs, this study is lacking direct observations for validation. Nevertheless, simulated *E. coli* concentrations in CSOs and effluents match well with observations in different areas from previous studies. In addition, the detailed temporal and spatial impact of CSO pollution is given by the model simulation. Given that direct and continuous monitoring of *E. coli* in CSO outfalls and receiving waters is challenging and costly, the model outputs offer a complementary dataset to observations in better understanding the *E. coli* dynamics during CSO-driven pollution events. However, *E. coli* removal efficiency in WWTPs was described as a function of influent flow, with high stormwater contributions reducing removal efficiency (van Heijnsbergen et al., 2022). In this study, a conservative constant *E. coli* reduction rate was used, representing wet-weather removal efficiency and potentially overestimating *E. coli* load in effluents during dry-weather conditions. Future applications should improve the coupling between the emission and rainfall-runoff models to enable dynamic simulation of *E. coli* reduction rates.

Process-based models are essential for assessing the impacts of future changes (de Brauwere et al., 2014; van der Meulen et al., 2024). Most of the existing process-based models have been applied to individual

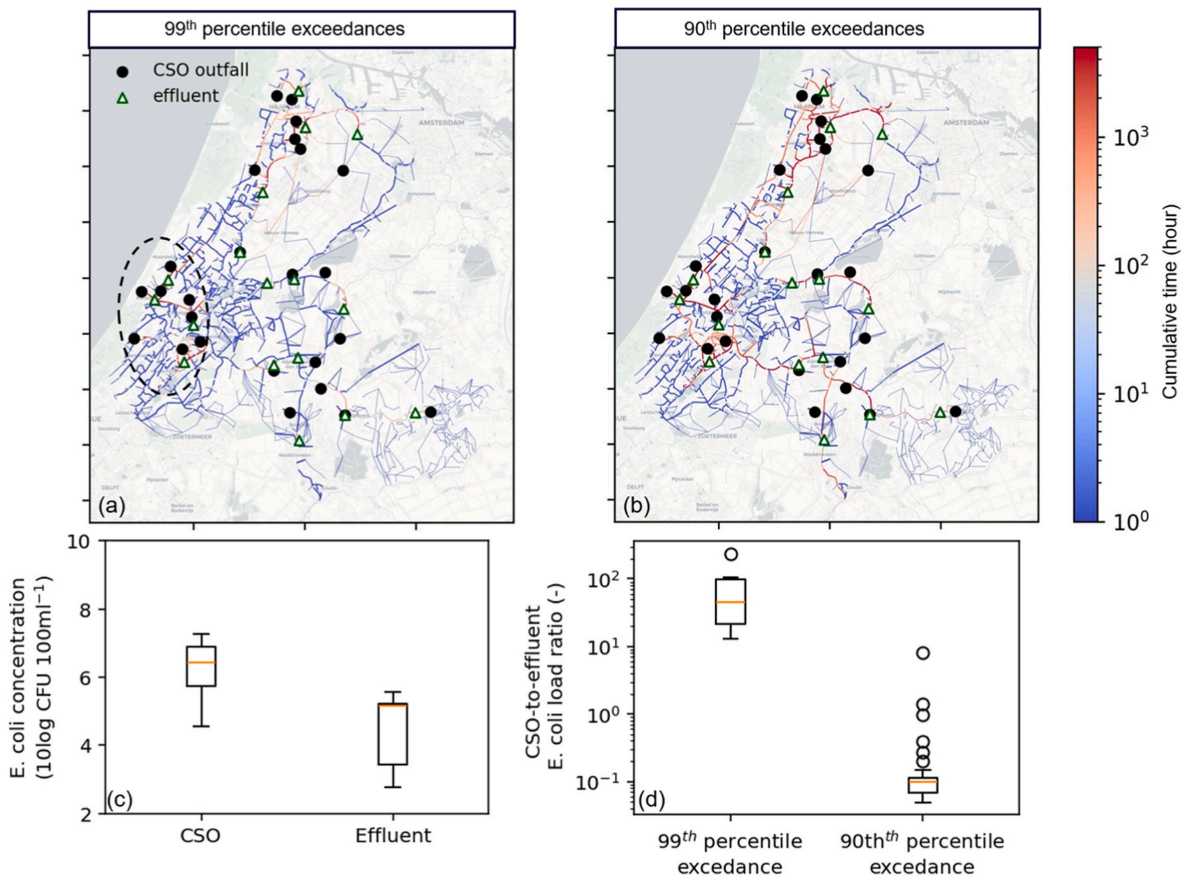

Fig. 5. Distribution of cumulative duration of 99th percentile exceedances (a) and 90th percentile exceedances (b) over the entire simulation period from 2017 to 2019. Black dots and green triangles denote the locations of CSO outfalls and effluents. The black dashed circle outlines the CSO outfalls and effluent discharge points adjacent to the inland water outlet, which are used for the ratio calculation (d). Aggregated ranges of *E. coli* concentrations in CSOs and effluents (c), and ratios of *E. coli* loads from CSOs and effluents during 99th and 90th percentile exceedances at the inland water outlet (d). All ranges were calculated over the entire simulation period (2017 – 2019). (For interpretation of the references to colour in this figure legend, the reader is referred to the Web version of this article.)

Fig. 6. Plume of *E. coli* pollution (exceedance of 500 CFU 100 ml^{-1}) duration in 2017 (a), 2018 (b) and 2019 (c).

waterbodies, such as river catchments (Kim et al., 2017; Ouattara et al., 2013), lakes (Bravo et al., 2017; Thorndahl et al., 2024) or coastal areas (Eregno et al., 2018; Gao et al., 2015). As a result, the continuity of pollution dynamics and cumulative effects from upstream to downstream are often neglected, constraining the power of such process-based models in future scenario projections. Adopting a source-to-sea modelling framework can improve system-level representation by explicitly capturing pollutant transport and transformation across connected aquatic compartments. This concept has been applied to modelling nutrients and the carbon cycle in aquatic continuums (Zepernick et al., 2023). To our knowledge, this is the first attempt to apply it in modelling microbial pollution. Climate change is expected to affect microbial water quality globally, yet quantitative future projections remain scarce (Hofstra, 2011). Source-to-Sea modelling combined with scenario-based simulations can translate these impacts into future microbial pollution risks at beaches and assess mitigation strategies for evidence-based policy-making.

4. Conclusion

A process-based source-to-sea model has been developed for an urban catchment and its downstream coastal waters, where CSO pollution is a major concern for the microbial water quality. The coupled model integrates an emission model, a rainfall-runoff model, an inland hydrology model, a coastal hydrodynamic model and a water quality model. Analysis of a three-year (2017 - 2019) simulation showed that.

1. With the simulation accuracy of 89%, the coupled model reliably reproduced the *E. coli* dynamics on the downstream beach and showed strong performance in representing peak concentrations based on CCDF analysis. In addition, the model enabled quantitative tracking of source contributions and identification of high pollution hotspots.
2. Simulated *E. coli* concentrations in CSO discharges across the catchment ranged from 4.6 to 7.3 ($\log_{10}$ CFU 100 ml^{-1}), in agreement with previously reported observations. This high variability indicates that a constant *E. coli* concentration commonly applied in earlier modelling studies may be insufficient to represent CSO microbial pollution.
3. 99th percentile exceedances at the inland water outlet were mainly caused by adjacent CSO emissions, whereas the 90th percentile exceedances reflected cumulative contributions along the stream.
4. The duration and spatial distribution of *E. coli* pollution on the beach result from the combined effects of inland *E. coli* load and coastal hydrodynamic conditions. The source-to-sea modelling framework effectively represents the pollution transport across the aquatic continuum.

The modelling framework developed in this study offers a generic approach for real-time forecasting in urban areas, particularly for assessing CSO-related pollution. By modelling pollution transport across the aquatic continuum, the framework provides a tool for investigating the impacts of future climate change on coastal microbial water quality.

CRediT authorship contribution statement

Hao Wang: Writing – original draft, Visualization, Methodology, Formal analysis, Data curation, Conceptualization. **Anouk Blauw:** Writing – review & editing, Supervision, Methodology, Conceptualization. **Jos van Gils:** Supervision, Methodology. **Eline Boelee:** Writing – review & editing, Supervision, Project administration, Funding acquisition. **Émile Sylvestre:** Writing – review & editing, Supervision, Methodology. **Gertjan Medema:** Writing – review & editing, Supervision.

Declaration of competing interests

The authors declare that they have no known competing financial interests or personal relationships that could have appeared to influence the work reported in this paper.

Acknowledgments

The authors thank Jan Jelle Reitsma and Johan Oosterbaan (Hoogheemraadschap van Rijnland) for support with the hydrological model setup and validation, and Theo van der Kaaij (Deltares) for assistance with the hydrodynamic model nesting. This research was supported through the BlueAdapt Project, funded by the European Union's Horizon Europe research and innovation programme under grant agreement No 101057764 and by the UKRI/HM Government.

Appendix A. Supplementary data

Supplementary data to this article can be found online at https://doi.org/10.1016/j.envpol.2026.129053.

Data availability

Data will be made available on request.

References

Al Aukidy, M., Verlicchi, P., 2017. Contributions of combined sewer overflows and treated effluents to the bacterial load released into a coastal area. Sci. Total Environ. 607, 483–496.
Barragán, J.M., De Andrés, M., 2015. Analysis and trends of the world's coastal cities and agglomerations. Ocean Coast Manag. 114, 11–20.
Belinda, J.K.E., van Onselen, Imke, Leenen, 2016. Haalbaarheidsstudie Bacterieerwijdering Blue Energy Centrale Katwijk. Arcadis.
Beyaard, L., Meszaros, L., Pathak, D., Christensen, K.H., Jamet, Q., Sperrevik, A.K., Kullman, I.K., Dumas, F., Pasquet, A., Brosse, F., Gourves, D., Cecilio, C., Bonanad, C., Almeida, L.P., Campuzano, F., Romão, S., Bellafiore, D., Ferrarin, C., She, J., Frishfelds, V., Schulz-Stellenfleth, J., Chen, W., Pein, J., Vieira da Silva, D., Jacob, B., Barnez Gramcianinov, C., Purayil, S.P., Legrand, S., Arneborg, L., Brunnabend, S.-E., Reyes Reyes, E., Navarro, M.G.-J., Jansen, E., Federico, I., Causio, S., Campanati, C., Mihailov, M.E., Garcia Hermosa, I., Johnson, K., Staneva, J., 2025. D6.1: implementation of CMEMS-MSCS interfaces. Zenodo.
Botturi, A., Ozbayram, E.G., Tondera, K., Gilbert, N.I., Rouault, P., Caradot, N., Gutierrez, O., Daneshgar, S., Frison, N., Akyol, Ç., 2021. Combined sewer overflows: a critical review on best practice and innovative solutions to mitigate impacts on environment and human health. Crit. Rev. Environ. Sci. Technol. 51, 1585–1618.
Bougeard, M., Le Saux, J.-C., Teillon, A., Belloir, J., Le Mennec, C., Thome, S., Durand, G., Pommepuy, M., 2011. Combining modeling and monitoring to study fecal contamination in a small rural catchment. J. Water Health 9, 467–482.
Bravo, H.R., McLellan, S.L., Klump, J.V., Hamidi, S.A., Talarczyk, D., 2017. Modeling the fecal coliform footprint in a Lake Michigan urban coastal area. Environ. Model. Software 95, 401–419.
Chan, S., Thoe, W., Lee, J., 2013. Real-time forecasting of Hong Kong beach water quality by 3D deterministic model. Water Res. 47, 1631–1647.
Chen, H., Chang, H., 2014. Response of discharge, TSS, and E. coli to rainfall events in urban, suburban, and rural watersheds. Environ. Sci. Process. Impacts 16, 2313–2324.
Cosby, A., Lebakula, V., Smith, C., Wanik, D., Bergene, K., Rose, A., Swanson, D., Bloom, D., 2024. Accelerating growth of human coastal populations at the global and continent levels: 2000–2018. Sci. Rep. 14, 22489.
de Brauwere, A., Ouattara, N.K., Servais, P., 2014. Modeling fecal indicator bacteria concentrations in natural surface waters: a review. Crit. Rev. Environ. Sci. Technol. 44, 2380–2453.
de Graaf, R., Van De Giesen, N., van de Ven, F., 2009. Alternative water management options to reduce vulnerability for climate change in the Netherlands. Nat. Hazards 51, 407–422.
Deltares, 2022. D-Flow flexible mesh user manual. Delta.
Deltares, 2023. D-Emissions: assessment tool for the emitted pollution at catchment scale. Delta.
Deltares, 2026. Sobek suite. Delta.
Derx, J., Müller-Thomy, H., Kılıç, H., Cervero-Arago, S., Linke, R., Lindner, G., Walochnik, J., Sommer, R., Komma, J., Farnleitner, A., 2023. A probabilistic-deterministic approach for assessing climate change effects on infection risks downstream of sewage emissions from CSOs. Water Res. 247, 120746.
Devane, M.L., Moriarty, E., Weaver, L., Cookson, A., Gilpin, B., 2020. Fecal indicator bacteria from environmental sources; strategies for identification to improve water quality monitoring. Water Res. 185, 116204.
Ellis, J., Butler, D., 2015. Surface water sewer misconnections in England and Wales: pollution sources and impacts. Sci. Total Environ. 526, 98–109.
Eregno, F.E., Tryland, I., Tjomsland, T., Kempa, M., Heistad, A., 2018. Hydrodynamic modelling of recreational water quality using Escherichia coli as an indicator of microbial contamination. J. Hydrol. 561, 179–186.
Erichsen, A.C., Kaas, H., Dannisøe, J., Mark, O., Jørgensen, C., 2006. Etablering af badevandsprofiler og varslingssystemer i henhold til EU's nye badevandsdirektiv. Miljøstyrelsen og DHI. Miljøprojekt.
EU, 2006. Directive 2006/7/EC of the european Parliament and of the Council concerning the management of bathing water quality and repealing directive 76/160/EEC. Off. J. Eur. Union.
EurEau, 2016. Overflows from Collecting Systems.
Gao, G., Falconer, R.A., Lin, B., 2015. Modelling the fate and transport of faecal bacteria in estuarine and coastal waters. Mar. Pollut. Bull. 100, 162–168.
Grace, M.J., Dickie, J., Bartie, P., Brown, C., Oliver, D.M., 2023. Understanding health outcomes from exposure to blue space resources: towards a mixed methods framework for analysis. Resources 12, 135.
Grasmeijer, B., Huisman, B., Luijendijk, A., Schrijvershof, R., Van Der Werf, J., Zijl, F., De Looff, H., De Vries, W., 2022. Modelling of annual sand transports at the Dutch lower shoreface. Ocean Coast Manag. 217, 105984.
Hofstra, N., 2011. Quantifying the impact of climate change on enteric waterborne pathogen concentrations in surface water. Curr. Opin. Environ. Sustain. 3, 471–479.
Ing, J., der Meulen, van, 2007. Zwemwaterkwaliteit katwijks kanaal. Hoogheemraadschap van Rijnland.
Islam, M.M., Sokolova, E., Hofstra, N., 2018. Modelling of river faecal indicator bacteria dynamics as a basis for faecal contamination reduction. J. Hydrol. 563, 1000–1008.
Jalliffier-Verne, I., Heniche, M., Madoux-Humery, A.-S., Galarneau, M., Servais, P., Prévost, M., Dorner, S., 2016. Cumulative effects of fecal contamination from combined sewer overflows: management for source water protection. J. Environ. Manag. 174, 62–70.
Kim, M., Boithias, L., Cho, K.H., Silvera, N., Thammahacksa, C., Latsachack, K., Rochelle-Newall, E., Sengtaheuanghoung, O., Pierret, A., Pachepsky, Y.A., Ribolzi, O., 2017. Hydrological modeling of Fecal Indicator Bacteria in a tropical mountain catchment. Water Res. 119, 102–113.

Lam, M.Y., Ahmadian, R., 2024. Enhancing hydro-epidemiological modelling of nearshore coastal waters with source-receptor connectivity study. Environ. Pollut. 345, 123431.

Locatelli, L., Russo, B., Acero Oliete, A., Sánchez Catalán, J.C., Martínez-Gomariz, E., Martínez, M., 2020. Modeling of E. coli distribution for hazard assessment of bathing waters affected by combined sewer overflows. Nat. Hazards Earth Syst. Sci. 20, 1219–1232.

Mattijs, H.F., Kleissen, Robert, van Cleef, Ultsje, van Gorkum, 2008. Maatregelenstudie Zwemwaterkwaliteit Katwijk. Rijkswaterstaat Noordzee.

Mohammed, M.H., Zwain, H.M., Hassan, W.H., 2021. Modeling the impacts of climate change and flooding on sanitary sewage system using SWMM simulation: a case study. Results Eng. 12, 100307.

Nie, L., Lindholm, O., Lindholm, G., Syversen, E., 2009. Impacts of climate change on urban drainage systems–a case study in Fredrikstad, Norway. Urban Water J. 6, 323–332.

Ouattara, N.K., de Brauwere, A., Billen, G., Servais, P., 2013. Modelling faecal contamination in the Scheldt drainage network. J. Mar. Syst. 128, 77–88.

Panidhapu, A., Li, Z., Aliashrafi, A., Peleato, N.M., 2020. Integration of weather conditions for predicting microbial water quality using Bayesian Belief networks. Water Res. 170, 115349.

Passerat, J., Ouattara, N.K., Mouchel, J.-M., Rocher, V., Servais, P., 2011. Impact of an intense combined sewer overflow event on the microbiological water quality of the Seine River. Water Res. 45, 893–903.

Penna, A., Marini, M., Ferrarin, C., Guicciardi, S., Grilli, F., Baldrighi, E., Ricci, F., Casabianca, S., Capellacci, S., Marinchel, N., 2023. Fecal bacteria contamination in the Adriatic Sea: investigating environmental factors and modeling to manage recreational coastal waters. Environ. Pollut. 338, 122700.

Perry, W.B., Ahmadian, R., Munday, M., Jones, O., Ormerod, S.J., Durance, I., 2024. Addressing the challenges of combined sewer overflows. Environ. Pollut. 343, 123225.

Peter, O.T., Siegersma, Heleen, de Man, 2023. Onderweg Naar Betere Zwemwaterkwaliteit Katwijk Aan Zee. Gemeente Katwijk.

Prinsen, G., Becker, B., 2011. Application of SOBEK hydraulic surface water models in the Netherlands Hydrological Modelling Instrument. Irrig. Drain. 60, 35–41.

Prinsen, G., Sperna Weiland, F., Ruijgh, E., 2015. The Delta model for fresh water policy analysis in the Netherlands. Water Resour. Manag. 29, 645–661.

Salerno, F., Gaetano, V., Gianni, T., 2018. Urbanization and climate change impacts on surface water quality: enhancing the resilience by reducing impervious surfaces. Water Res. 144, 491–502.

Searcy, R.T., Boehm, A.B., 2021. A day at the beach: enabling coastal water quality prediction with high-frequency sampling and data-driven models. Environ. Sci. Technol. 55, 1908–1918.

Seis, W., Veldhuis, M.-C.T., Rouault, P., Steffelbauer, D., Medema, G., 2024. A new Bayesian approach for managing bathing water quality at river bathing locations vulnerable to short-term pollution. Water Res. 252, 121186.

Semenza, J.C., 2020. Cascading risks of waterborne diseases from climate change. Nat. Immunol. 21, 484–487.

Servais, P., Garcia-Armisen, T., George, I., Billen, G., 2007. Fecal bacteria in the rivers of the Seine drainage network (France): sources, fate and modelling. Sci. Total Environ. 375, 152–167.

Servais, P., Poulin, M., Flipo, N., Lesage, L., Goncalves, A., Rocher, V., Masnada, S., Lucas, F., Mouchel, J.M., 2011. Vers Un Modèle De La Contamination Par Temps De Pluie En Seine.

Smeets, P.W.M.H., Rietveld, L.C., van Dijk, J.C., Medema, G.J., 2010. Practical applications of quantitative microbial risk assessment (QMRA) for water safety plans. Water Sci. Technol. 61, 1561–1568.

Sterk, A., de Man, H., Schijven, J.F., de Nijs, T., de Roda Husman, A.M., 2016. Climate change impact on infection risks during bathing downstream of sewage emissions from CSOs or WWTPs. Water Res. 105, 11–21.

Thorndahl, S., Nielsen, J.M., Rasmussen, M.R., 2024. Model-based prediction of bathing water quality in a lake polluted by fecal coliform bacteria from combined sewer overflows. J. Environ. Manag. 349, 119483.

Van der Brugge, R., Rotmans, J., Loorbach, D., 2005. The transition in Dutch water management. Reg. Environ. Change 5, 164–176.

van der Meulen, E., Tertienko, A., Blauw, A., Sutton, N., van de Ven, F., Rijnaarts, H., van Oel, P., 2024. A review of prediction models for E. coli in urban surface waters. Urban Water J. 21, 539–548.

van Heijnsbergen, E., Niebaum, G., Lämmchen, V., Borneman, A., Hernández Leal, L., Klasmeier, J.r., Schmitt, H., 2022. Antibiotic-resistant) E. coli in the Dutch–German Vecht catchment— monitoring and modeling. Environ. Sci. Technol. 56, 15064–15073.

Vermeulen, L.C., Hofstra, N., Kroeze, C., Medema, G., 2015. Advancing waterborne pathogen modelling: lessons from global nutrient export models. Curr. Opin. Environ. Sustain. 14, 109–120.

Wang, H., Blauw, A., van Gils, J., Boelee, E., Sylvestre, É., Medema, G., 2025. Development and evaluation of a physico-biochemical model for Escherichia coli in bathing waters. Water Res., 125199

Zepernick, B.N., Wilhelm, S.W., Bullerjahn, G.S., Paerl, H.W., 2023. Climate change and the aquatic continuum: a cyanobacterial comeback story. Environmental Microbiology Reports 15, 3–12.

Zhang, J., Qiu, H., Li, X., Niu, J., Nevers, M.B., Hu, X., Phanikumar, M.S., 2018. Real-Time nowcasting of microbiological water quality at recreational beaches: a wavelet and artificial neural network-based hybrid modeling approach. Environ. Sci. Technol. 52, 8446–8455.

Zijl, F., Laan, S., Emmanouil, A., van Kessel, T., van Zelst, V., Vilmin, L., van Duren, L., 2021. Potential Ecosystem Effects of Large Upscaling of Offshore Wind in the North Sea. Deltares, Delft, The Netherlands.

Zijl, F., Sumihar, J., Verlaan, M., 2015. Application of data assimilation for improved operational water level forecasting on the northwest European shelf and North Sea. Ocean Dyn. 65, 1699–1716.

Zijl, F., Verlaan, M., Gerritsen, H., 2013. Improved water-level forecasting for the Northwest European Shelf and North Sea through direct modelling of tide, surge and non-linear interaction. Ocean Dyn. 63, 823–847.